Rare Metal Materials and Engineering
Volume 54, Issue 12, December 2025
Available online at www.rmme.ac.cn

Science Press

Cite this article as: Zheng Deyu, Xia Yufeng, Zhou Jie. Microstructure Homogenization Control of GH4706 Alloy by Hot Deformation Maps[J]. Rare Metal Materials and Engineering, 2025, 54(12): 3000-3009. DOI: https://doi.org/10.12442/j.issn.1002-185X.20240716.

ARTICLE

Microstructure Homogenization Control of GH4706 Alloy by Hot Deformation Maps

Zheng Deyu, Xia Yufeng, Zhou Jie

Chongqing Key Laboratory of Advanced Mold Intelligent Manufacturing, School of Materials Science and Engineering, Chongqing University, Chongqing 400044, China

Abstract: Hot compression tests for GH4706 alloy were performed at a true strain of 1.2 within the temperature range of 950–1150 °C and the strain rate range of 0.001–1 s^{-1}. The optimal hot deformation temperature and strain rate range were determined using nephogram maps of dynamic recrystallization fraction, average grain size, and grain distribution standard deviation. Processing maps at true strains from 0.4 to 0.9 were generated based on flow stress curves to identify the strain corresponding to optimal microstructure homogenization efficiency at various temperatures and strain rates. Results show that within the optimal parameter range, under the conditions of 1150 °C and 0.01 s^{-1}, the true strain of about 0.6 results in the optimal microstructure homogenization efficiency. The grain orientation spread maps obtained from the experiment also confirms this conclusion. This study provides an effective method for microstructure homogenization control of GH4706 alloy and an effective reference for the minimum strain threshold of the local part of the forging in engineering.

Key words: GH4706 alloy; dynamic recrystallization; microstructure; homogenization efficiency; processing map

1 Introduction

GH4706 (IN706) alloy is a typical Ni-Fe-Cr alloy with excellent cold and hot formability, fine creep resistance, and good oxidation resistance, which is suitable for hot segment aero-engine components, such as turbine disks, blades, and shells[1–3]. The microstructure of GH4706 alloy should be homogeneous and refined to ensure the service life of forgings in the extreme environment of aviation and the nuclear industry[4]. To achieve this goal, homogenous grain structure of GH4706 alloy must be obtained through the dynamic recrystallization (DRX) process during hot deformation[5]. However, the flow behavior of GH4706 alloy is very sensitive to processing parameters, such as strain, temperature, and strain rate, which constrains the suitable processing parameters into narrow hot working windows[6]. For the superlarge forgings of nickel-based alloys[7], the cost of the traditional trial-and-error method for the identification of processing parameters is unacceptable. Therefore, it is necessary to find an effective method to optimize the processing parameters and microstructure of GH4706 alloy.

It is widely accepted that hot deformation maps, which contain nephogram and processing map, are valuable for the selection of optimal processing parameters across a wide range of strains, strain rates, and temperatures[6–9]. Prasad et al[10] developed the processing map based on the dynamic material model (DMM). According to DMM theory, the power dissipation efficiency (η) is calculated from the distribution of strain rate sensitivity (m) with deformation temperature and strain rate, which characterizes the metallurgical mechanism distribution at a given temperature and strain. Recently, the hot processing map has been widely used to determine the hot working parameters and to regulate the corresponding microstructure[11]. Huang et al[6] developed the hot deformation maps for GH4706 alloy at true strain of 0.7, temperature of 900–1150 ℃, and strain rate of 0.001–1 s^{-1}. They found that the optimal hot working conditions are 940–970 ℃ and 0.015–0.003 s^{-1}, providing reference for the future applications of GH4706 alloy. However, with more harsh requirements about the size and performance for GH4706 alloy forgings, it is essential to further

Received date: December 02, 2024
Foundation item: National Key R&D Program Project (2022YFB3705103)
Corresponding author: Xia Yufeng, Ph. D., Professor, Chongqing Key Laboratory of Advanced Mold Intelligent Manufacturing, School of Materials Science and Engineering, Chongqing University, Chongqing 400044, P. R. China, E-mail: yufengxia@cqu.edu.cn

optimize the parameter window for superlarge forgings.

It is well known that the higher the strain, the more favorable the DRX nucleation. This is because with the increase in strain, the dislocation density and stored energy are increased[12]. Although DRX degree rises with strain, DMM theory[10] demonstrates that the power efficiency of microstructure rebuilding should be considered, which is confirmed by the typical nonlinear relationship between DRX evolution and strain[13]. Additionally, Huang et al[8] demonstrated that when the strain increases during hot deformation, the area of the ideal process window firstly increases and subsequently declines. This phenomenon indicates that there is a DRX efficiency inflection point as the strain increases. Thus, it is imperative to take into account the effect of strain on DRX efficiency, namely microstructure homogenization efficiency.

The purpose of this study is to identify the ideal range for hot deformation temperature and strain rate using nephogram maps of DRX results. The optimal strain, which is defined as the strain related to optimal microstructure homogenization efficiency, was also identified by drawing processing maps of the GH4706 alloy. This study provided an effective method for microstructure homogenization control of GH4706 alloy. Meanwhile, this research also provided an effective reference for the minimum strain threshold of the local part of the forging in engineering.

2 Experiment

The material used in this study was forged GH4706 alloy, and the isothermal hot compression tests were conducted on a computer-controlled hydraulic Gleeble-1500 thermal simulator. The samples were cut into the ones with diameter of 8 mm and height of 15 mm by wire-electrode cutting. To reduce the anisotropy of flow behavior, each sample was heated to the designed deformation temperature at a heating rate of 10 ℃/s and maintained for 180 s. The deformation temperature range was 950 – 1150 ℃ with the increment of 50 ℃, and the strain rates were 0.001, 0.01, 0.1, and 1 s^{-1}. The true strain of compression test was 1.2. The deformed samples were quenched in water immediately after compression test. In addition, six samples were compressed at 1150 ℃/0.01 s^{-1} under strain of 0.4 – 0.9 to verify the optimal strain. The true stress and true strain curves were recorded. The electron backscattered diffraction (EBSD) observations were conducted in the middle area of the cutting samples by JSM 7800F scanning electron microscope (SEM). EBSD samples were ground by 3000# silicon carbide sandpaper and then electropolished in an electrolyte solution of 10vol% $HClO_4$ and 90vol% C_2H_5OH at 22 V for 20 s. The prepared samples were stored in an alcohol solution. Fig. 1 shows the initial microstructure of forged GH4706 alloy.

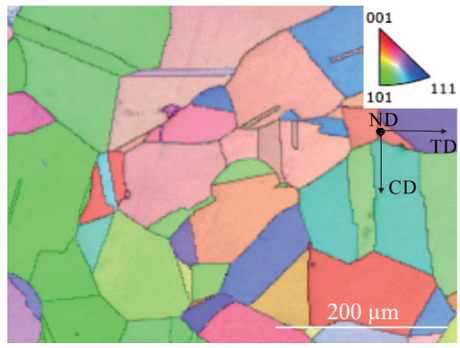

Fig.1 Initial microstructure of forged GH4706 alloy (ND is normal direction; TD is transverse direction; CD is compression direction)

3 Computing Method

3.1 Processing map theory

Based on the dynamic material model (DMM)[10], the total power consumption P of the material during compression is related to the flow stress and strain rate, including two complementary parts. The first part is the power consumption G due to temperature rise, and the second part is the power consumption J of microstructure evolution. The relationship between G and J can be expressed as Eq.(1), as follows:

$$P = \sigma\dot{\varepsilon} = \int_0^{\dot{\varepsilon}} \sigma \mathrm{d}\dot{\varepsilon} + \int_0^{\sigma} \dot{\varepsilon} \mathrm{d}\sigma = G + J \tag{1}$$

where σ is the stress, and $\dot{\varepsilon}$ is the strain rate. The ratio between G and J is denoted as m to reflect the sensitivity of stress to strain rate at a certain temperature T and a certain strain ε. Thus, m can be expressed as Eq.(2):

$$m = \left.\frac{\partial J}{\partial G}\right|_{T,\varepsilon} = \frac{\partial J}{\partial P}\frac{\partial P}{\partial G} = \frac{\sigma \mathrm{d}\dot{\varepsilon}}{\dot{\varepsilon}\mathrm{d}\sigma} = \left.\frac{\partial \ln\sigma}{\partial \ln\dot{\varepsilon}}\right|_{T,\varepsilon} \tag{2}$$

The relationship between stress and strain rate can be expressed in the power law form of m:

$$\sigma = K\dot{\varepsilon}^m \tag{3}$$

where K is the undetermined constant. By substituting Eq.(3) into Eq.(1), Eq.(4–5) of J and G are obtained, respectively:

$$J = \frac{m\sigma\dot{\varepsilon}}{m+1} \tag{4}$$

$$G = \frac{\sigma\dot{\varepsilon}}{m+1} \tag{5}$$

The power dissipation efficiency of microstructure evolution η is the ratio of the actual dissipation J to the ideal dissipation J_{ideal} ($J_{\mathrm{ideal}} = 0.5\sigma\dot{\varepsilon}$) when m=1. Thus, η is also a function of m:

$$\eta = \frac{J}{J_{\mathrm{ideal}}} = \frac{2m}{m+1} \tag{6}$$

To avoid the fluctuation of power dissipation parameters caused by material flow instability, it is specified that the material has flow instability when the entropy generation rate in the metallurgical system reaches the maximum value. Based on this assumption, the plastic flow instability[14] is shown in Eq.(7), as follows:

$$\frac{\partial \ln J}{\partial \ln\dot{\varepsilon}} < 1 \tag{7}$$

The expression of $\xi(\dot{\varepsilon})$ can be obtained by substituting Eq. (4) into Eq. (7), and $\xi(\dot{\varepsilon}) < 0$ is defined as the instability criterion:

$$\xi(\dot{\varepsilon}) = \frac{\partial \ln\left(\frac{m}{m+1}\right)}{\partial \ln \dot{\varepsilon}} + m < 0 \quad (8)$$

The ideal microstructure control is realized through the superposition of the power dissipation map and the instability map to establish the processing map.

3.2 Standard deviation of grain size distribution

The average grain size and DRX fraction response maps can directly reflect the quantitative relationship between microstructure and parameters[15]. However, it cannot reflect the grain size distribution.

The standard deviation of grain size distribution S is used to express the fluctuation of grain size to further quantify the grain size distribution, as shown in Eq.(9):

$$S = \sqrt{\frac{\sum_{i=1}^{n}\left(x_i - \bar{x}\right)^2}{n}} \quad (9)$$

where n is the number of grains; x_i and $\bar{x}$ are the diameter of the ith grain and the average grain diameter, respectively. The larger the S value, the greater the fluctuation of grain size. On the contrary, the smaller the S value, the more uniform the grain size distribution.

4 Experiment Results and Analysis

4.1 Flow stress curves

Fig. 2a – 2d show the true stress-true strain curves of GH4706 alloy under the deformation temperature range of 950–1150 °C and the strain rate range of 0.001–1 s^{-1} when the samples are compressed to the true strain of 1.2 (true strain of 1.2 is the average strain of GH4706 alloy superlarge forging). There is a substantial relationship among stress, temperature, strain rate, and strain. The stress is increased with the increase in strain rate and the decrease in temperature. The flow stress increases rapidly at small strain, then increases slowly with the deformation, and finally tends to be stable. DRX process includes two processes[16]: nucleation (interface formation) and growth (interface migration), which determine the grain refinement and coarsening, respectively. The evolution shape of the true stress-true strain curve is determined by the competitive result between nucleation and growth[17].

4.2 Microstructure distribution at strain of 1.2

Fig. 3[15] shows the microstructures of GH4706 alloy deformed to strain of 1.2 at temperature of 950–1150 °C and strain rate of 0.001 – 1 s^{-1}. It can be observed that the microstructures dominated by equiaxed grains (new DRX grains) are distributed below the red solid line A-A (high temperature and low strain rate), whereas the microstructures dominated by deformed grains (original grains) are distributed above the red solid line A-A (low temperature and high strain rate). Below 1100 °C, equiaxed grains can only be obtained by reducing the strain rate to below 0.01 s^{-1}; whereas above 1100 °C, equiaxed grains are easier to obtain and less affected by strain rate, as shown in Fig. 3s and 3t. However, excessively high temperature and low strain rate can also promote the grain growth, as shown in Fig. 3q and 3r. Since the temperature can promote the grain boundary migration[16], the microstructure exhibits strong work hardening or dynamic recovery characteristics as the temperature decreases. The strain rate promotes the nucleation of DRX, because DRX process is mainly controlled by high nucleation at high strain

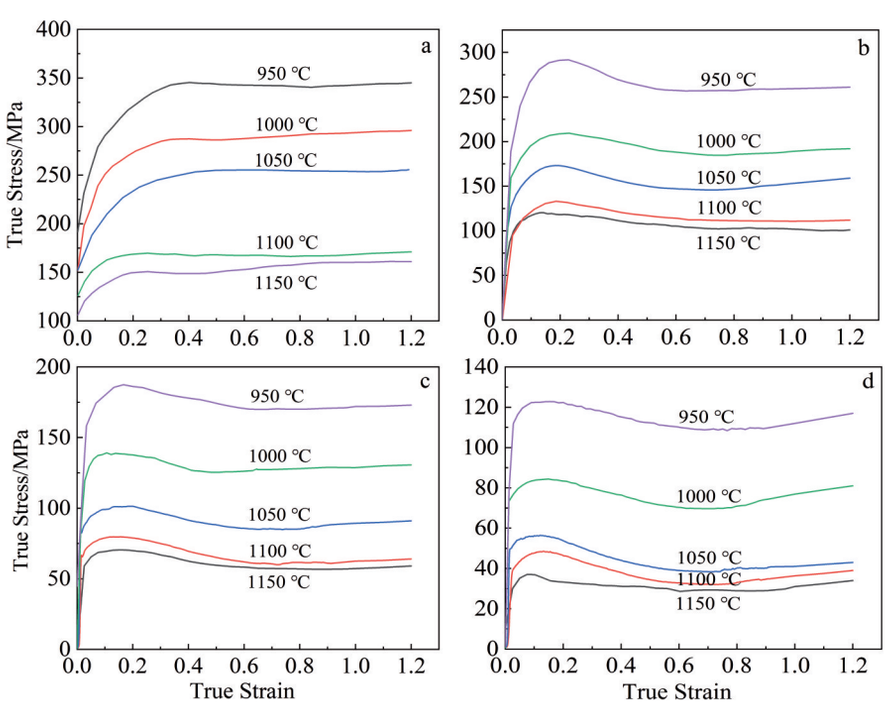

Fig.2 Flow stress curves at different strain rates: (a) 1 s^{-1}, (b) 0.1 s^{-1}, (c) 0.01 s^{-1}, and (d) 0.001 s^{-1}

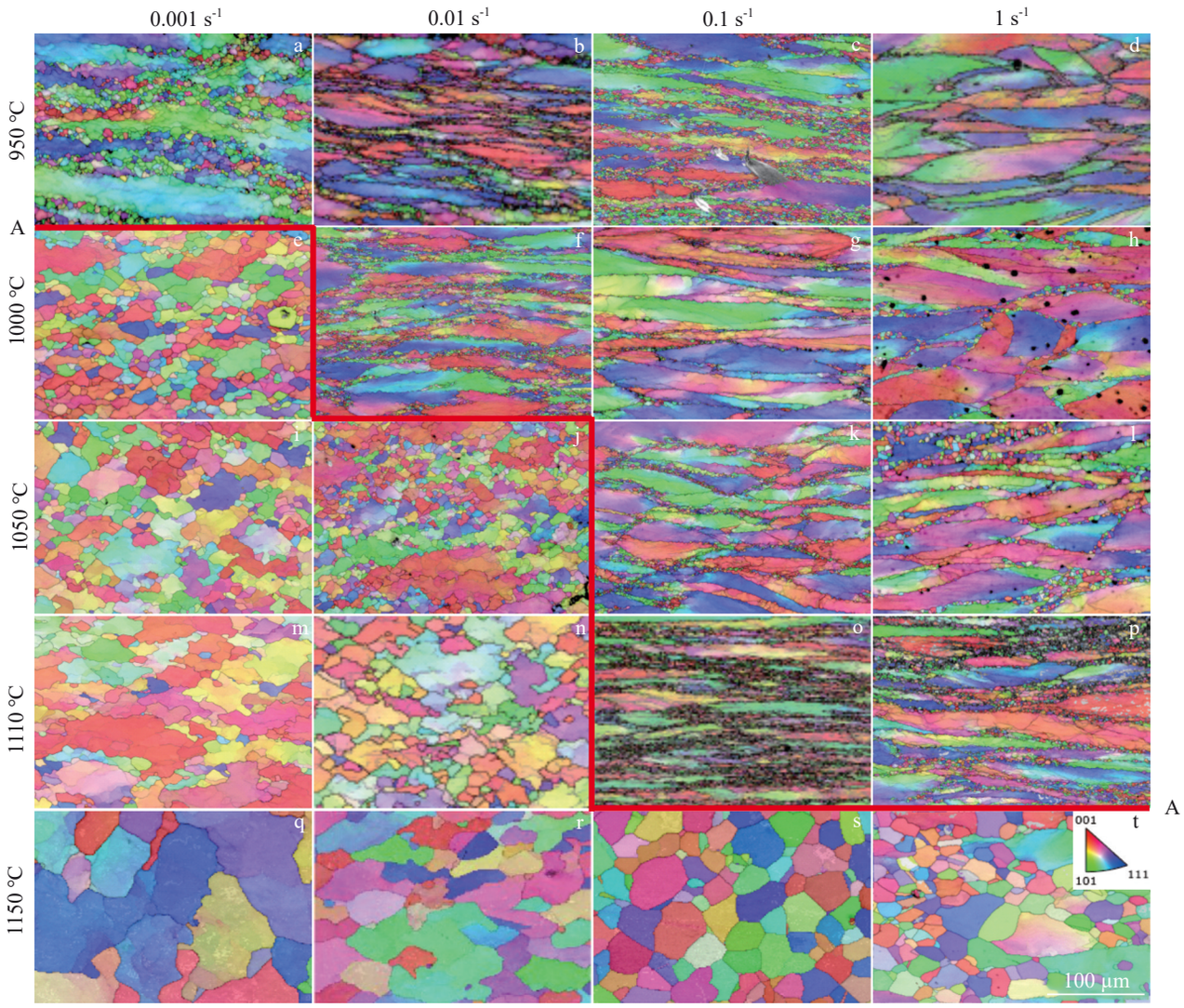

Fig.3 Microstructures of GH4706 alloy deformed at different temperatures and strain rates[15]

rates[17]. Due to the short growth time of equiaxed grains, finer equiaxed grains will be obtained, as shown in Fig. 3h and 3l. Therefore, as the strain rate increases, there will be more equiaxed grains around the deformed grains, exhibiting a typical discontinuous DRX microstructure, namely the necklace microstructure. When the strain rate decreases, equiaxed grains will gradually replace the original deformed grains due to sufficient deformation time, as shown in Fig. 3e and 3i, indicating that lower strain rates can accelerate the microstructure homogenization process.

4.3 Nephograms at strain of 1.2

Based on the properties of GH4706 alloy, it is important to analyze how DRX behavior responds to different process parameters to achieve the ideal homogenous equiaxed microstructure. The hot deformation map can reflect the relationship between hot deformation behavior and parameters[6]. The nephograms of DRX fraction, average grain size, and grain distribution standard deviation at true strain of 1.2 are shown in Fig. 4a – 4c, respectively. The average grain size and the grain distribution standard deviation are decreased with the increase in DRX fraction. These responses do not exhibit a straightforward monotonic relationship with temperature and strain rate, which highlights the intricacy of DRX process. Average grain size decreases as a result of the progressive replacement of the original grains by newly generated DRX equiaxed grains during hot deformation. High temperatures will reduce grain boundaries and boost grain growth, both of which will increase the average grain size. The extremely nonlinear growth of average grain size is determined by the relationship between grain coarsening and refinement during DRX evolution[18]. Generally, sufficient DRX time at low or medium strain rates can yield the optimal microstructure. However, low strain rates and high temperatures will cause the grains to grow quickly. An excessively low strain rate may cause the grain to expand and reduce production efficiency, and an excessively high strain rate combined with extremely low temperature will cause overload and damage to the equipment. Therefore, according to the comprehensive consideration of three maps and in combination with the forging load, two ideal parameters regions are determined: region A (1100 – 1150 °C/0.01 – 0.1 s^{-1}) and region B (960 –

1010 °C/0.001–0.01 s^{-1})[6–7].

4.4 Evolution of strain rate sensitivity response map with strain

The strain rate sensitivity m of flow stress reflects the sensitivity level of flow stress to strain rate, which is a very important parameter to describe the behavior in the hot forming process and also an important physical parameter to reflect the microstructure evolution mechanism[8–10]. Polynomial fitting was performed on the logarithm of stress and strain rate to obtain the true response of m to the parameters of strain, strain rate, and temperature during hot deformation. m for each parameter was determined according to the slope of the corresponding point of the spline, as shown in Fig.5a–5f.

The value of m reflects the ratio of J to G, as shown in Eq.(2). The term G represents the power dissipated by plastic work, most of which is converted into heat, and the remaining is stored as lattice defects[10]. This phenomenon indicates that the G term is a parameter related to grain coarsening or deterioration. The J term is related to the metallurgical mechanism of dynamic generation with power dissipation, which means J is a relevant parameter of grain refinement. There is a dynamic competitive relationship between J and G for refinement, coarsening, optimization, and deterioration of grains. This complex mechanism shows the nonlinear relationship between strain and microstructure reconstruction efficiency. Therefore, the competition between J and G at a certain strain according to the value of m[8–11] can be evaluated. The cubic spline interpolation operation is performed on the m value, and the three-dimensional response surface maps of m under true strains of 0.4–0.9 are obtained, as shown in Fig.6a–6f. It can be found that in the evolution process of m, the regions with higher value are almost located in the region A and region B, as well as the transition position between them. With the increase in strain, the m value of the region B is increased and it is always higher than that of the region A. The change of m value indicates that there are different hot deformation mechanisms[8]. At strain of 0.4, the m value in the region A is below 0.3, which is a typical feature of dislocation slip or

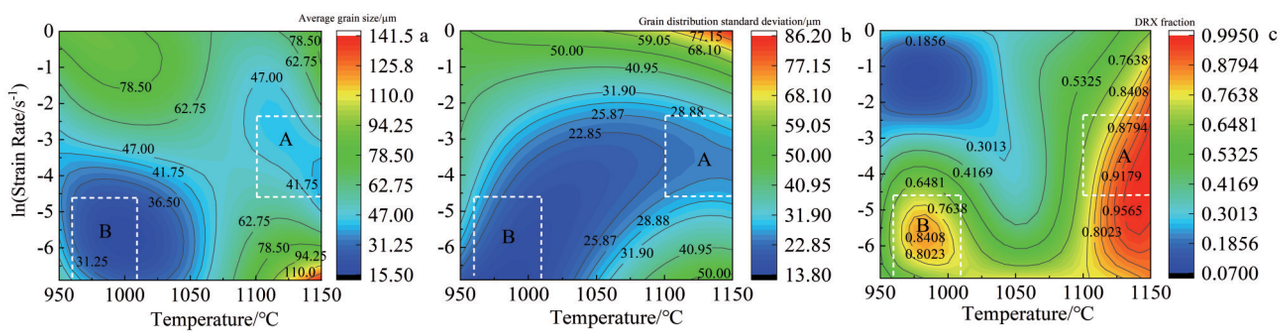

Fig.4 Nephograms of average grain size (a), grain size distribution standard deviation (b), and DRX fraction (c) of GH4706 alloy

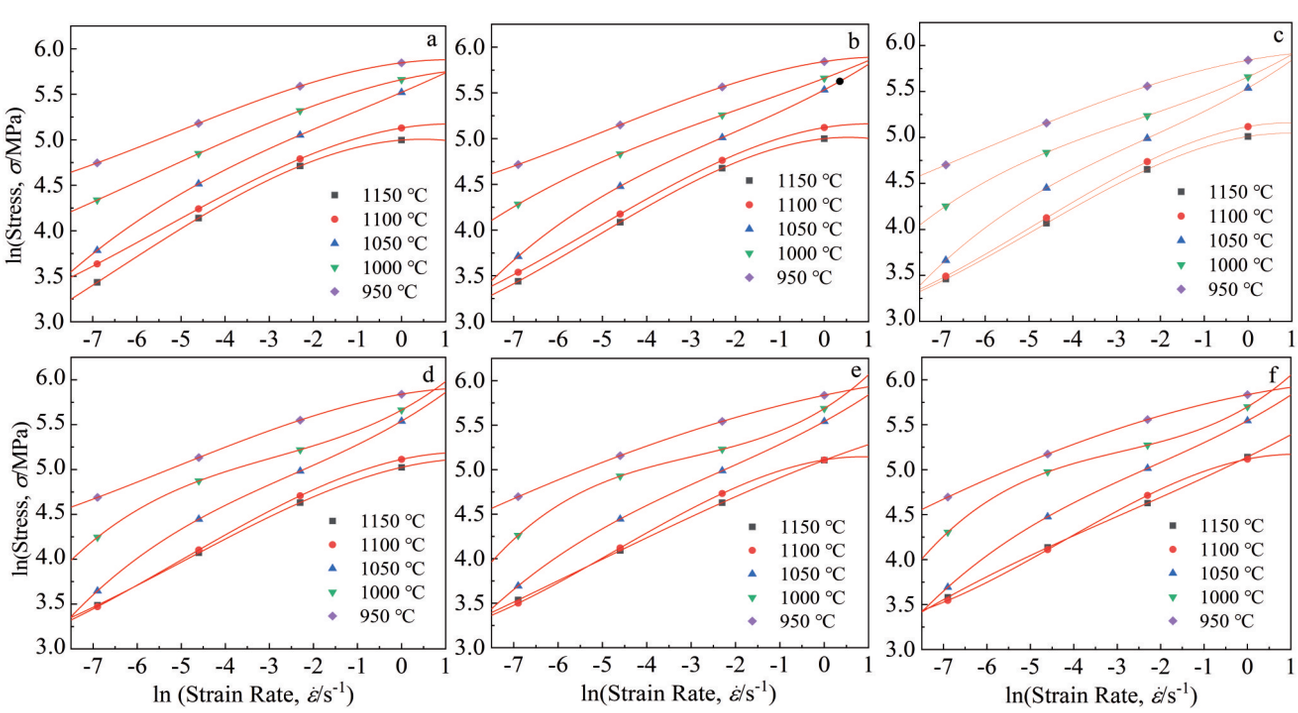

Fig.5 Relationships between stress and strain rate at true strain of 0.4 (a), 0.5 (b), 0.6 (c), 0.7 (d), 0.8 (e), and 0.9 (f)

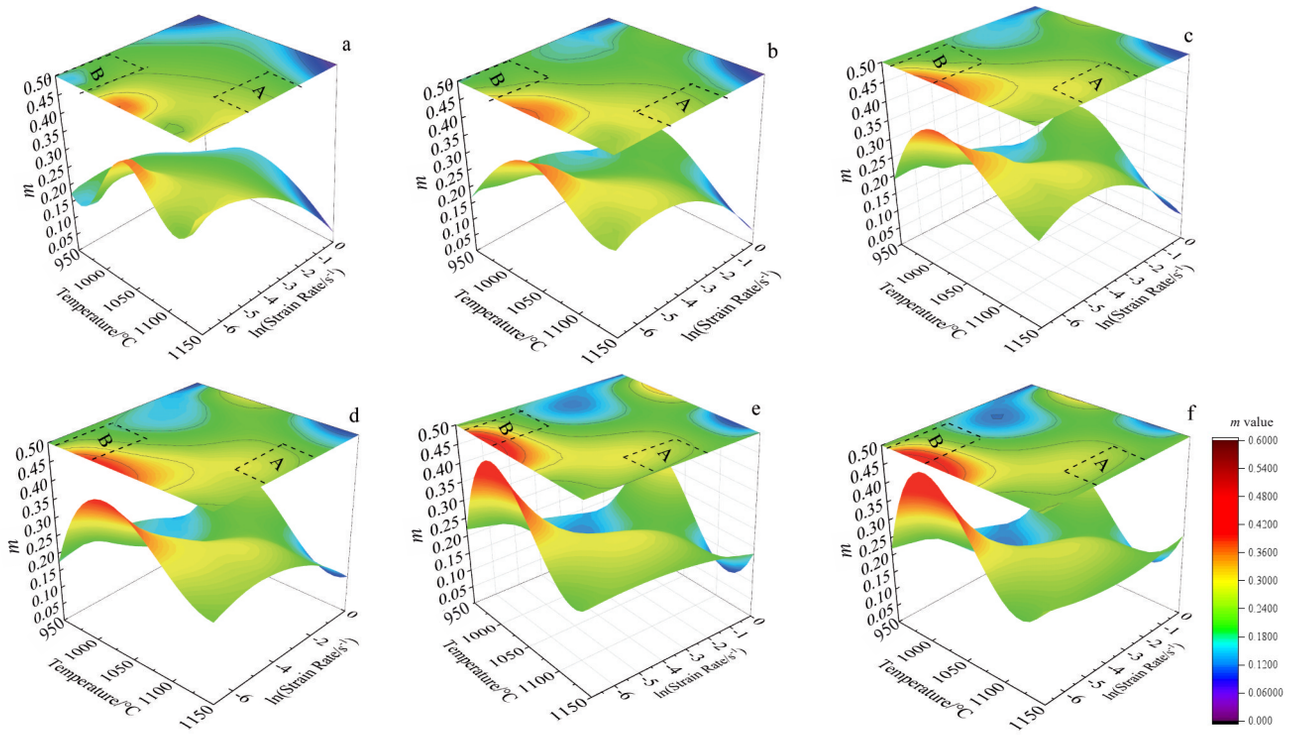

Fig.6 3D results of *m* value at true strain of 0.4 (a), 0.5 (b), 0.6 (c), 0.7 (d), 0.8 (e), and 0.9 (f)

climb-limited slip belonging to the power-law creep mode[19]. The *m* value in the center of the region B is above 0.32, which means that DRX behavior begins[11]. As the strain continues to increase, the basal slip, non-basal slip, and twin plastic deformation mechanisms are combined, and the *m* value continues to increase[20]. It should be noted that the power dissipation efficiency of hot working, such as DRX, is lower than 0.5, because the power dissipation occurs through the formation of interfaces generated by dislocation rearrangement and recovery[14]. In the center of the region B, there is an *m* value exceeding 0.5, which means that there is a risk of crack initiation[10,14]. The evolution of *m* in the region A is always related to DRX mechanism, so the temperature and strain rate in region A are optimal for DRX behavior. According to the distribution maps of *m* value, the area related to DRX mechanism reaches the maximum when the strain reaches 0.6, and it gradually decreases when the strain exceeds 0.6. This result can be further confirmed from the evolution of the power dissipation efficiency value η.

4.5 Evolution of instability region with strain

The instability map is the response of the ξ value to temperature and strain rate at a certain strain, where the ξ characteristic value is negative[9]. According to Eq. (8), the ξ value is the slope of the logarithmic curve, which is obtained by the polynomial fitting method. Thus, ξ values were calculated and the results are shown in Fig.7. The cubic spline interpolation operation was conducted to plot the response maps of the ξ value to temperature and strain rate at true strains of 0.4 – 0.9, and the results are shown in Fig. 8. The unstable state and stable state regions are distinguished by gray and white colors, respectively.

As shown in Fig.8a–8c, the instability region at strain of 0.4–0.6 occurs at the position of high strain rate, and the instability originates from local shear or twinning, resulting in the reduction of slip[21]. When the strain exceeds 0.6, as shown in Fig.8d–8f, the instability region also appears near the region B, and the area of instability region is gradually increased with the increase in strain. Using the parameters from the instability region at low temperature and medium strain rate, the prepared samples generally show coarse-grain structures, which may be due to the abnormal grain growth or precipitation during deformation[14]. GH4706 alloy produces the second precipitation, such as Ni_3Ti, at low temperature, but the precipitation will dissolve at high temperatures. Ref. [22] reported that the solute resistance effect will interfere with the dynamic recovery mechanism and adversely affect the formability of materials. Therefore, it can be concluded that the parameters in region A are in the optimal parameter range.

4.6 Evolution of processing maps with strain

The processing map is the superposition of the instability map and the power dissipation map, which can reveal the deterministic region of the metallurgical process and the limit conditions of flow instability[7–9]. Dynamic recovery and DRX are considered as good metallurgical mechanisms, whereas voids, cracks, adiabatic shear bands, and dynamic strain aging are considered as bad mechanisms, which lead to microstructure deterioration[20]. Therefore, the evolution of the microstructure mechanism of the hot deformation system can be obtained by processing maps at different strains. Power dissipation value η characterizes the evolution mechanism of

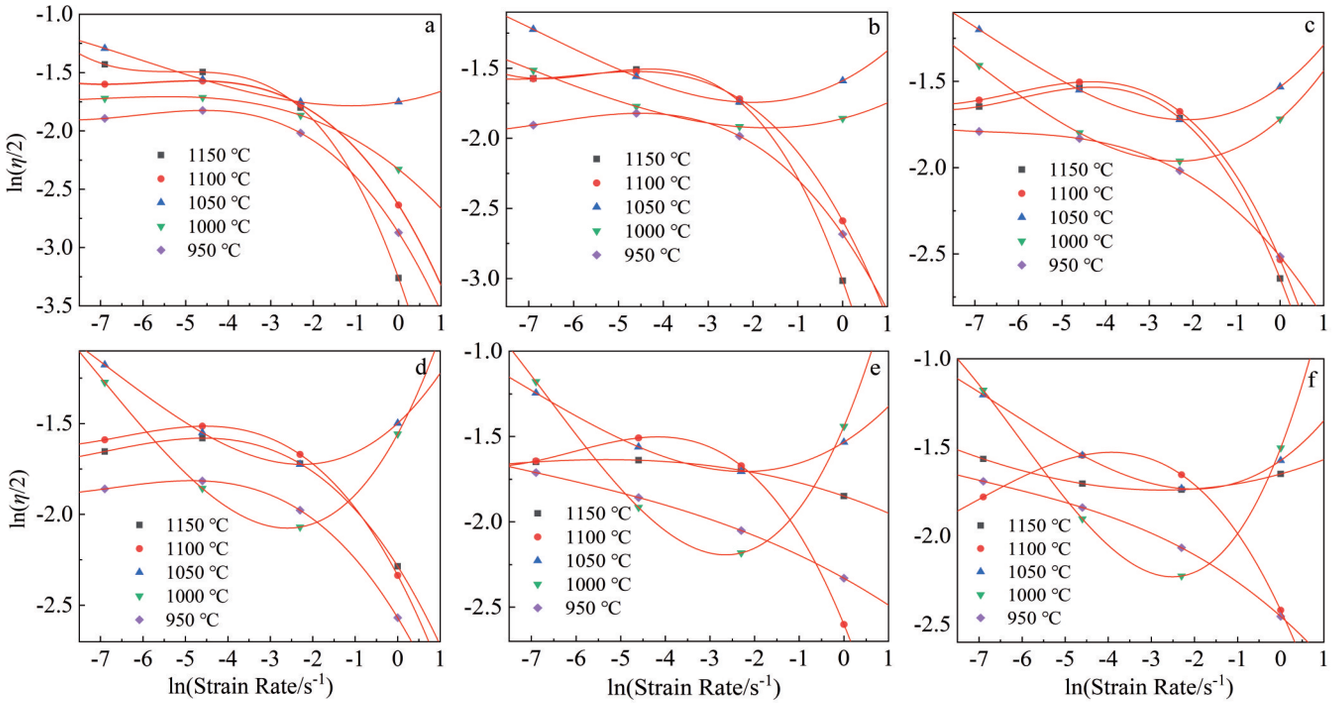

Fig.7 Relationship between ln(η/2) and strain rate at true strain of 0.4 (a), 0.5 (b), 0.6 (c), 0.7 (d), 0.8 (e), and 0.9 (f)

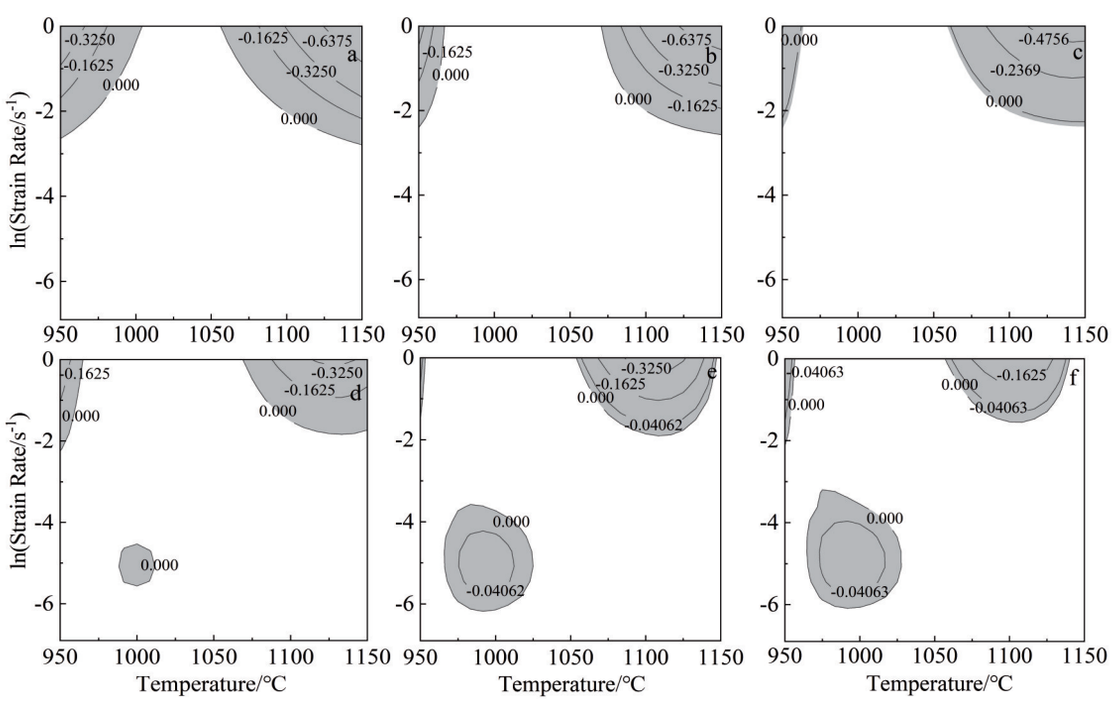

Fig.8 Instability maps of GH4706 alloy at true strain of 0.4 (a), 0.5 (b), 0.6 (c), 0.7 (d), 0.8 (e), and 0.9 (f)

microstructure during hot deformation. Researches show that the η value of the cracking process is usually very high, because the efficiency of converting power into surface energy is the highest. Therefore, generally, η>0.50[14]. When the power dissipation occurs with the interfaces generated by DRX and the dislocation rearrangement, the efficiency is at the medium level of 0.30< η <0.45[14]. Within this range, the larger the η value, the better the microstructure homogenization efficiency. The η value is 0.2–0.3 when the dynamic recovery behavior begins[7–9]. In addition, the efficiency peak in each region can either represent the lowest power dissipation or the highest entropy generation rate[11].

The η values were calculated according to the m value and then interpolated by a cubic spline. The response maps of η to temperature and strain rate at true strains of 0.4–0.9 are obtained and superimposed with the instability maps, as shown in Fig. 9.

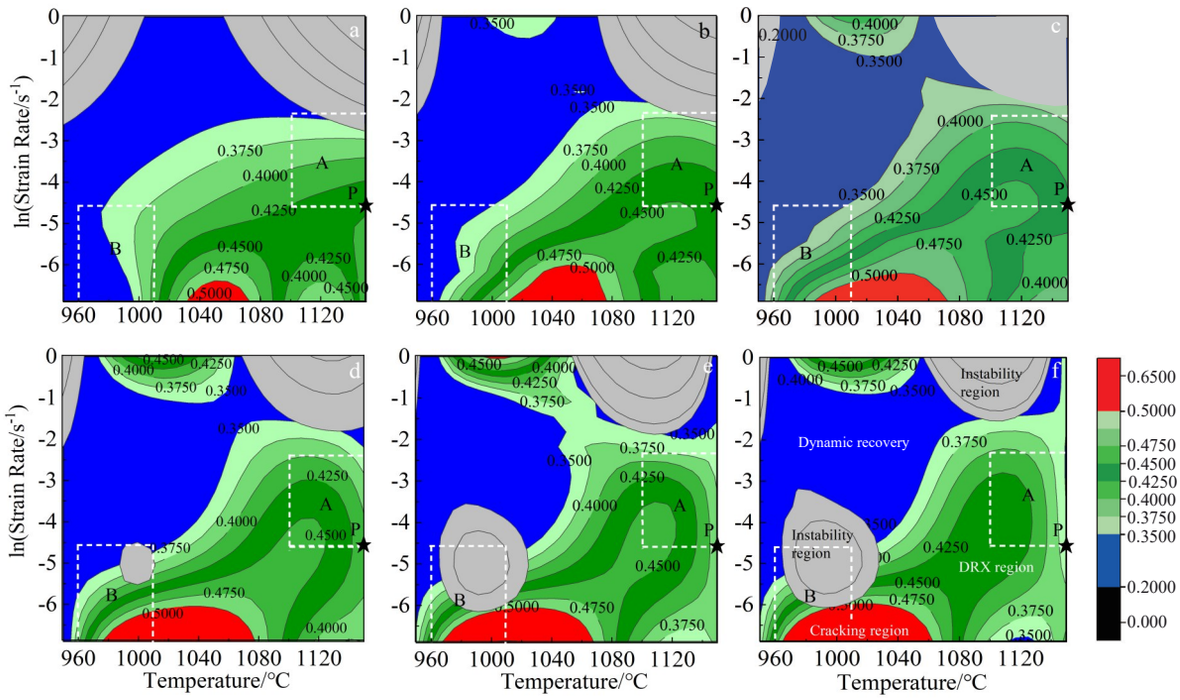

Fig.9 Processing maps of GH4706 alloy at true strain of 0.4 (a), 0.5 (b), 0.6 (c), 0.7 (d), 0.8 (e), and 0.9 (f)

Clearly, η contour shapes change at different strains. Different shades of green color are used to express η. The darker the green shade, the better the microstructure homogenization efficiency. Accordingly, the optimal strain range can be approximately determined by the area contained within the area of isolines between 0.40 and 0.45 in the region A. DRX starts in most area of the region A, but a small instability area appears at the upper right corner, which leads to the risk of microstructure deterioration for forgings (Fig. 9a–9b). As the strain increases to 0.6 (Fig. 9c), DRX becomes the sole mechanism. Therefore, the microstructure of large forgings will not deteriorate at strain of 0.6 when the parameters are within the region A. As shown in Fig. 9d – 9f, DRX is the sole mechanism. However, with the increase in strain, the microstructure homogenization efficiency is decreased, especially using the parameters from the right side of region A (the recrystallization fraction on the right side is higher). Besides, when the strain is 0.7, the instability region and the cracking region appear near the region B. The method of processing maps can be used to determine the optimal strain under the certain parameters. For example, the η value at point P (1150 °C and 0.01 s^{-1}) is decreased from 0.450 to 0.425 with the increase in strain from 0.6 to 0.7, and it further decreases to 0.375 with the further increase in strain to 0.9. Therefore, the strain of 0.6 is related to the optimal microstructure homogenization efficiency at temperature of 1150 °C and strain rate of 0.01 s^{-1}.

5 Microstructure Observation and Verification

5.1 Verification of optimal temperature region and strain rate region

Grain orientation spread (GOS) maps were used to characterize the microstructure of different regions (region A: 1150 °C/0.01 s^{-1}; region B: 1000 °C/0.01 s^{-1}; dynamic recovery region: 1000 °C/0.1 s^{-1}) in the processing map at true strain of 1.2, as shown in Fig. 10. The average grain size, DRX fraction, and grain distribution standard deviation are shown in Fig. 10d. The microstructure of the region A shows fully recrystallized and well-developed uniform grains. However, it can be found that the grain has grown to a certain degree, which is caused by high temperature and low strain rate[13]. A typical imperfect recrystallization structure with some non-recrystallized deformed grains can be seen in the microstructure of the region B in Fig. 10b. This result verifies that the parameters in region B are also suitable for DRX behavior, but the microstructure homogenization efficiency is much lower, compared with that using the parameters in the region A. The microstructure of dynamic recovery region shows a deformed structure. Therefore, the feasibility of the proposed processing map to define the optimal parameter range is verified.

5.2 Verification of optimal strain

GOS maps were also used to characterize the microstructure evolution at point P (1150 °C and 0.01 s^{-1}) in the region A under different strain conditions, as shown in Fig. 11. It can be found that with the increase in true strain, the microstructure gradually shows the characteristics of uniformity and refinement. This result reflects the typical strain-induced DRX mechanism[12]. The original microstructure has been replaced and reconstructed by DRX structure at a certain strain. The statistic results of average grain size, DRX fraction, and grain distribution standard deviation at different strains are shown in Fig. 11g – 11i. The variation trends of average grain size and DRX fraction are

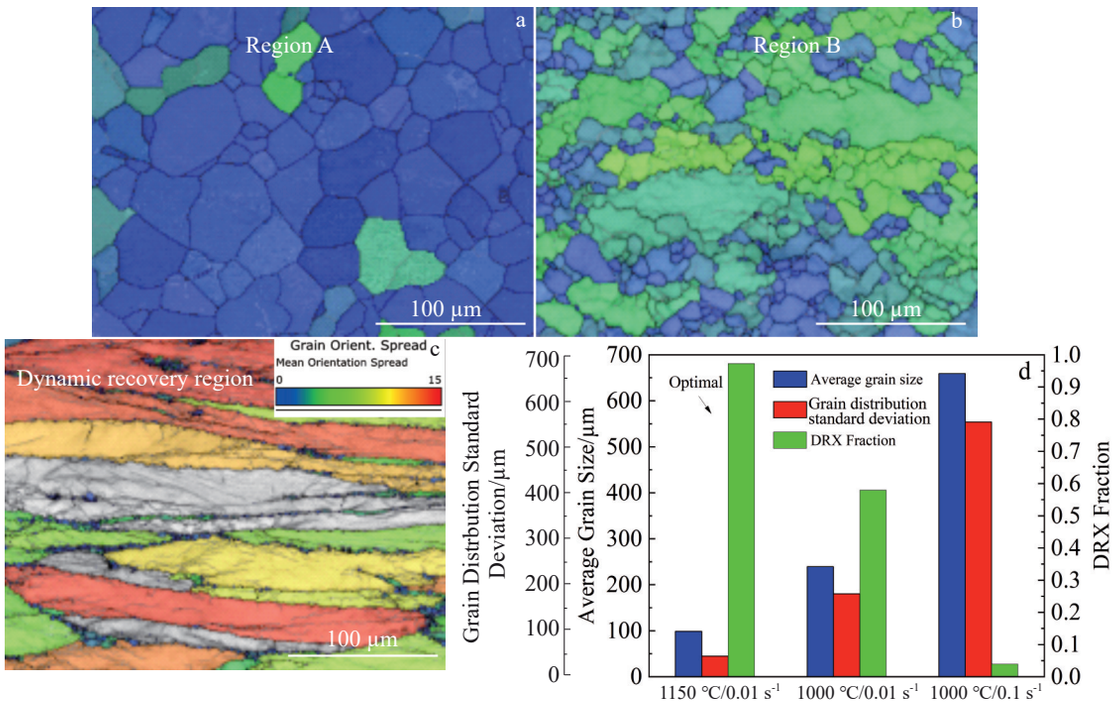

Fig.10 GOS maps of GH4706 alloy under deformation conditions of 1150 ℃/0.01 s^{-1} (a), 1000 ℃/0.01 s^{-1} (b), and 1000 ℃/0.1 s^{-1} (c); DRX analysis results of GH4706 alloy under different conditions (d)

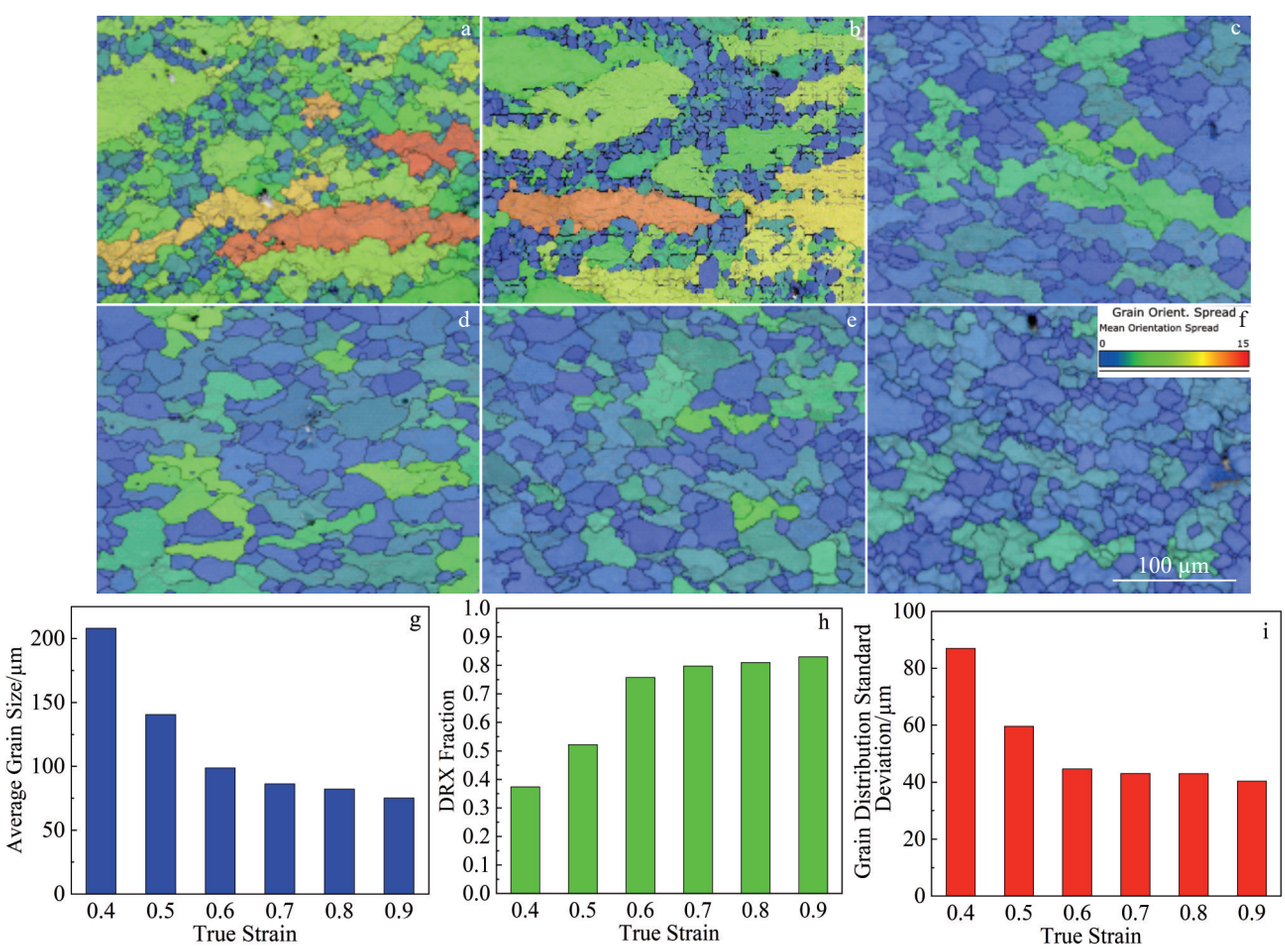

Fig.11 GOS maps of GH4706 alloy at true strain of 0.4 (a), 0.5 (b), 0.6 (c), 0.7 (d), 0.8 (e), and 0.9 (f); average grain size (g), DRX fraction (h), and grain distribution standard deviation (i) of GH4706 alloy at different true strains

opposite within the strain range of 0.4–0.9, which is consistent with the typical DRX evolution characteristics[15]. When the true strain exceeds 0.6, the change rate of average grain size, DRX fraction, and grain distribution standard deviation tend to be obviously gentle. This phenomenon means that the true strain of 0.6 is related to the optimal microstructure homogenization efficiency, which is consistent with the conclusion of the processing map and further confirms the accuracy of the processing map. Thus, the hot deformation at temperature of 1150 ℃ and strain rate of 0.01 s^{-1} can result in the optimal microstructure homogenization efficiency at the strain of 0.6. This conclusion can provide a theoretical basis for the strain homogenization design of GH4706 forgings and an effective reference for the minimum strain threshold of the local part of the forging in engineering.

6 Conclusions

1) The hot deformation at temperature of 1150 ℃ and strain rate of 0.01 s^{-1} can result in the optimal microstructure homogenization efficiency at the strain of 0.6. The proposed processing map can be used to determine the optimal strain at different temperature and strain rate conditions.

2) This study provides an effective method for microstructure homogenization control of GH4706 alloy. Meanwhile, it can also provide an effective reference for the minimum strain threshold of the local part of the forging in engineering.

References

1 Sharma P, Chakradhar D, Narendranath S. *Materials and Design*[J], 2015, 88: 558

2 Ferro P, Zambon A, Bonollo F. *Materials Science and Engineering A*[J], 2005, 392: 94

3 Mukherji D, Gilles R, Barbier B *et al. Scripta Materialia*[J], 2003, 48: 143

4 Wang G Q, Chen M S, Li H B *et al. Journal of Materials Science & Technology*[J], 2021, 77: 47

5 Zhang B Y, Wang Z T, Yu H *et al. Journal of Alloys and Compounds*[J], 2022, 900: 163515

6 Huang S, Wang L, Lian X T *et al. International Journal of Minerals, Metallurgy and Materials*[J], 2014, 21: 462

7 Zheng D Y, Xia Y F, Teng H H *et al. Rare Metal Materials and Engineering*[J], 2024, 53(7): 1887

8 Huang Shuhai, Zhao Zude, Xia Zhixin *et al. Rare Metal Materials and Engineering*[J], 2010, 39(5): 848 (in Chinese)

9 Zeng Weidong, Zhou Yigang, Zhou Jun *et al. Rare Metal Materials and Engineering*[J], 2006, 35(5): 673 (in Chinese)

10 Prasad Y V, Gegel H L, Doraivelu S M *et al*. *Metall Trans A*[J], 1984, 15: 1883

11 Shen J Y, Hu L X, Sun Y *et al*. *Journal of Alloys and Compounds*[J], 2020, 822: 153735

12 Li X W, Sun H F, Zhang P *et al*. *Intermetallics*[J], 2014, 55: 90

13 Huang K, Logé R E. *Materials and Design*[J], 2016, 111: 548

14 Srinivasan N, Prasad Y V, Rao R P. *Materials Science and Engineering A*[J], 2008, 476: 146

15 Zheng D Y, Xia Y F, Zhang S F *et al*. *Journal of Plasticity Engineering*[J], 2025, 32(5): 143

16 Huo Y M, Huo C L, He T *et al. Journal of Materials Engineering and Performance*[J], 2024, 33: 9893

17 Li L, Wang Y, Li H *et al. Computational Materials Science*[J], 2019, 166: 221

18 Quan G Z, Wen Z H, Shen L *et al. Materials Reports*[J], 2021, 35: 18154

19 Luo J, Wang L F, Liu S F *et al. Materials Science and Engineering A*[J], 2016, 654: 213

20 Quan G Z, Ku T W, Song W J *et al. Materials and Design*[J], 2011, 32: 2462

21 Prasad Y V R K. *Journal of Materials Engineering and Performance*[J], 2003, 12: 638

22 Wang M J, Wang W R, Liu Z L *et al. Materials Today Communications*[J], 2018, 14: 188

基于热变形图方法的GH4706合金微观组织均匀化控制

郑德宇，夏玉峰，周　杰

(重庆大学 材料科学与工程学院 先进模具智能制造重庆市重点实验室，重庆 400044)

摘　要：GH4706合金在950~1150 ℃的温度范围内和0.001~1 s^{-1}的应变率范围内，在1.2的真应变下进行了热压缩试验。使用动态再结晶分数、平均晶粒尺寸和晶粒分布标准偏差的云图确定了最佳热变形温度和应变率范围。基于流动应力曲线绘制了0.4~0.9真应变下的加工图，以确定在不同温度和应变率下最佳微观组织均匀化效率相对应的应变。结果表明：在最佳参数范围内，在1150 ℃和0.01 s^{-1}条件下，约为0.6的真应变具有最高的微观组织均匀化效率。实验获得的晶粒取向扩展图证明了此结论。本研究为GH4706合金的微观组织均匀化控制提供了一种有效的方法，为确定工程中锻件局部最小应变阈值提供了有效参考。

关键词：GH4706合金；动态再结晶；微观组织；均匀化效率；加工图

作者简介：郑德宇，男，1983年生，博士，重庆大学材料科学与工程学院先进模具智能制造重庆市重点实验室，重庆 400044，E-mail：13193805@qq.com